ELSEVIER

Journal of Chromatography A, 779 (1997) 165–183

JOURNAL OF CHROMATOGRAPHY A

Recycling electrophoretic separations: modeling of isotachophoresis and isoelectric focusing

J.C. Baygents*, B.C.E. Schwarz, R.R. Deshmukh, M. Bier

Department of Chemical and Environmental Engineering, University of Arizona, Tucson, AZ 85721, USA

Received 3 September 1996; received in revised form 6 November 1996; accepted 6 November 1996

Abstract

The conventional, one-dimensional model that is the foundation for the dynamic simulation of electrophoretic separations is modified to describe the essential features of recycling electrophoresis instruments. Simulations are performed for the isoelectric focusing (IEF) and the isotachophoresis (ITP) modes. Results are compared with experimental data from prototype recycling free-flow IEF and ITP devices. Agreement between the experiments and the simulations is favorable, though electrode and electroosmotic effects, which are omitted from the model, are noticeable in the IEF instrument. Three parameters relevant to the design of recycling electrophoresis devices, viz. the number of ports for the recycle manifold, the residence time in the separation chamber per cycle, and the current density, are investigated with the model. © 1996 Elsevier Science B.V

Keywords: Isotachophoresis; Isoelectric focusing; Simulated electrophoresis; Recycling electrophoresis; Proteins; Albumin; Haemoglobin

1. Introduction

Electrophoretic separations involve the resolution of mixtures of ionized solutes into discernible sub-populations by the application of an electric field. Species within the mixture are resolved into the various sub-populations, at least in part, on the basis of their electrophoretic mobility.

Electrophoresis is eminently feasible and useful on the analytical scale, as indicated by the popularity of the myriad forms of gel and capillary electrophoresis. However, the scale up of electrophoretic devices to accommodate larger volumes for downstream bioprocessing is inherently problematic, owing to Joule heating, as well as to the occurrence of electroosmotic and electrohydrodynamic flows. As the volume of a separation chamber grows, the ability to thermostat the fluid diminishes and deleterious thermal effects ensue (e.g., natural convection). Similar problems arise if one attempts to increase the separation rate in smaller chambers by imposing stronger electric fields.

Nevertheless scale up of isoelectric focusing (IEF) and isotachophoresis (ITP) has been accomplished by carrying out separations in free fluids, without gels or other supporting matrices. Rapid recycling of the process fluids permits external dissipation of Joule heat, but requires careful streamlining of the flow. Fig. 1 illustrates this principle schematically. The buffer and separands (e.g., proteins) are introduced at the bottom of the separation chamber through an input manifold and removed similarly at

*Corresponding author.

0021-9673/97/$17.00
PII S0021-9673(96)00963-6

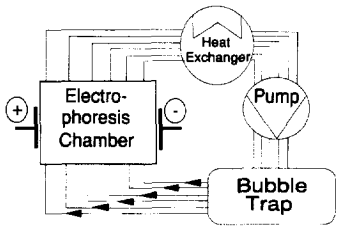

Fig. 1. Schematic diagram of the major components in a typical recycling electrophoresis device.

the chamber top. While in the cell, the solution is subject to an electric field, which is imposed orthogonal to the fluid motion; the axis of the separation is thus perpendicular to the flow. On exit from the separation chamber, the liquid passes through a heat exchanger and a bubble trap. The bubble trap also serves as a reservoir that helps to keep the chamber volume small. The heat exchanger permits temperature control and allows for the imposition of high voltage gradients, which are necessary for reasonable separation rates.

Various devices that use a recycling feature have been successfully implemented over the past two decades. The recycling isoelectric focusing apparatus was the first instrument to employ the principle [1]. The recycling IEF separation chamber is divided into compartments by nylon monofilament screens to streamline the fluid motion and the (batch) device has the capacity to process proteins at a rate of 1–5 g/h. A smaller instrument, called the ROTOFOR (Bio-Rad Labs., Hercules, CA, USA), uses a cylindrical separation chamber rotated on its horizontal axis, and partitioned by the nylon screens [2], to achieve the same results. It is cooled by an inner concentric cylinder filled with coolant. Two large-scale preparative instruments, the RF3 [3] and a recycling ITP device [4], employ a narrow rectangular channel with rapid flow for the electrophoresis chamber; instead of monofilament screens, however, a rapid recycling flow is used to suppress unwanted convection. The capacity of these two instruments is about 100–500 ml and 1 g/h can be processed. Another device, called the MinipHor (Protein Technologies, Tucson, AZ, USA), also uses a narrow, rectangular channel with rapid flow. The MinipHor is designed for IEF and has a capacity of approximately 30 ml.

The IsoPRIME apparatus (Hoefer, San Francisco, CA, USA [5,6]) and the Gradiflow [7,8] are preparative scale instruments that also employ recycling of the process fluid through the separation chamber, which for these devices is divided into subcompartments by membranes. Due to differences in their electrically-driven transport across the membranes, the separands are fractionated into the various subcompartments and separation is thus achieved.

Electrophoretic separations, such as IEF and ITP, involve some physicochemical interactions between the buffer constituents and the separands. For example, IEF depends on the natural development of a pH gradient upon the imposition of the electric field; the development of the pH gradient is a strong function of the chemistry of the buffer components. As a consequence, mathematical simulations of electrophoretic separations provide a means to evaluate the utility of specific buffer systems as media in which to carry out a given separation. Moreover, for recycling separations, the simulations can be used as a design tool for optimizing residence times, recycle rates, the number of channels in the input and output manifold, device control and automation, etc., and for predicting the device throughput and the final position of the separands along the separation axis.

A general model to describe the classical modes of electrophoretic separation was developed by Bier et al. [9], and integrated into a dynamic electrophoresis simulation program [10]. Subsequent improvements to the model included the treatment of the amphoteric behavior of proteins in IEF [11], and the introduction of artificial dispersion terms [12] to make numerical simulation of higher current densities possible, as has been demonstrated for isotachophoresis and zone electrophoresis [13]. However these dynamic simulations are formulated in one spatial dimension and omit consideration of effects, such as mixing in the recycle loop, that arise due to the repeated cycling of the fluids through the separation chamber. Thus the extant simulations are not directly suited to recycling devices and yield inadequate descriptions of their dynamic behavior [4].

In this paper we apply the general electrophoresis model so as to account for recycling and make limited comparisons of the model to experimental

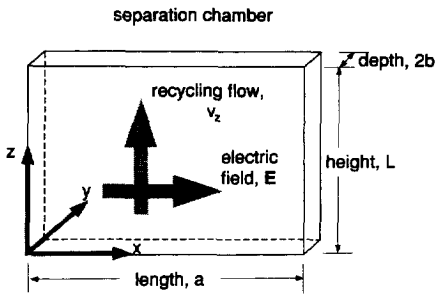

Fig. 2. Definition sketch for a recycling electrophoresis chamber. The electric field is applied in the x-direction, the recycling flow is in the z-direction.

data obtained from prototype recycling IEF and ITP instruments. As depicted in Fig. 2, the recycling flow in such devices is orthogonal to the separation axis, so at the outset, the problem involves at least two spatial dimensions. By making several simplifying approximations, and by adopting a (Lagrangian) frame of reference wherein we follow fluid through the separation chamber, we find that recycling can influence the separation in predominantly two ways. First, the temporal evolution of the concentration fields is protracted by the amount of time the fluid spends outside of the separation chamber. Second the spatial distribution of constituents is altered by mixing in the recycle loop. This mixing is manifested as dispersion of solutes along the separation axis. So, by design, this effect must be made secondary in order for the recycling device to work (e.g., a satisfactory fractionation will not occur with too few ports in the recycle manifold).

The presentation begins with the mathematical model, which, as alluded to above, consists of the well-established balance laws applied to a separation chamber such as that shown in Fig. 2. We then discuss the experiments to which the results of several IEF and ITP simulations are compared. Thereafter, we undertake a series of parametric studies whereby we examine the effect of three features related to the design and operation of recycling electrophoresis devices: the number of tubes used to transport the fluids around the recycle loop; the fraction of cycle time spent in the separation chamber; and the operating current density. Of the results shown, perhaps the most significant for preparative IEF or ITP is that the time to carry out the separation grows dramatically if the capacity of the separation chamber becomes too small relative to the volume of fluid being processed.

2. Mathematical model

A general set of balance laws describing electrophoretic separations, developed in the early to mid-1980s [9,10,14–17], has been detailed in a recent monograph by Mosher et al. [18]. Subject to the constraints of charge conservation and Maxwell's equations, these balance laws account for: one, the transport of ionic and neutral solutes (e.g., hydrogen ions, ampholytes and proteins) due to diffusion, electromigration and convection; and two, ionogenic (dissociation–association) reactions involving the solutes. The independent variables in the model are position $\mathbf{x}$ and time t and the dependent variables are the electric potential ϕ, the concentrations of the buffer constituents n_k ($k=1, 2, ..., N$), and the concentration of the separands n_{N+j} ($j=1, 2, ..., M$). The velocity $\mathbf{v}$ that drives the convective transport is presumed known.

Below we summarize the balance laws, assuming that the M separands are proteins and that the N buffer constituents are H^+, OH^- and various amphoteric species. Our notation follows that of Mosher et al. [18]. We then take up the treatment of recycling, where we assume that, as they are convected around the recycle loop, the solutes are mixed over the cross-sections of the individual recycle tubes.

2.1. The balance laws

Owing to the disparity between the Debye screening length of the ionic solution and the length scale associated with the separations process, electroneutrality prevails locally, viz.

$$0=\sum_{k=1}^{N} z_k n_k + \sum_{j=1}^{M} z_{N+j} n_{N+j} \tag{1}$$

The first sum on the right-hand side of Eq. (1) arises from the charge associated with H^+, OH^- and the

other buffer species, where z_k is the valence of species k. The second sum is contributed by the proteins. The effective valence of the jth protein is

$$z_{N+j} = z_j^0 - \bar{\nu}_j, \quad j = 1, 2, ..., M, \tag{2}$$

where z_j^0 is the valence of a molecule of protein j that contains all k_j of its dissociable protons and $\bar{\nu}_j$ is the average number of protons that are dissociated. The extent of dissociation varies locally with the hydrogen ion concentration according to the ratio

$$\bar{\nu}_j = \frac{\sum_{i=1}^{k_j} i(n_1)^{-i} \prod_{m=1}^{i} K_m^{(j)}}{1 + \sum_{i=1}^{k_j} (n_1)^{-i} \prod_{m=1}^{i} K_m^{(j)}}, \quad j = 1, 2, ..., M, \tag{3}$$

where $n_1 = [H^+]$ and $K_m^{(j)}$ is the equilibrium constant for the mth proton dissociation of protein j.

It follows from Eq. (1) that charge conservation requires

$$0 = \nabla \cdot \mathbf{i}_e = e\nabla \cdot \sum_{k=1}^{N} z_k \mathbf{f}_k + \nabla \cdot \mathbf{i}_p, \tag{4}$$

where $\mathbf{i}_e$ is the electric current density, $\mathbf{f}_k$ is the flux of species k, viz.

$$\mathbf{f}_k = \mathbf{v}n_k - ez_k\omega_k n_k \nabla\phi - k_B T \omega_k \nabla n_k, \quad k = 1, 2, ..., N, \tag{5}$$

and $\mathbf{i}_p$ is the density of the current carried by the proteins. In Eq. (5), $k_B T$ is the Boltzmann temperature and ω_k is the mobility of species k. If ω_{N+j}, the mobility of protein j, is independent of the protein's ionization, then

$$\nabla \cdot \mathbf{i}_p = -\nabla \cdot \{e^2 \sum_{j=1}^{M} \omega_{N+j}[(z_j^0)^2 - 2\bar{\nu}_j z_j^0 + \overline{\bar{\nu}_j^2}] n_{N+j} \nabla\phi + ek_B T \sum_{j=1}^{M} \omega_{N+j} \nabla(z_{N+j} n_{N+j})\}, \tag{6}$$

with

$$\overline{\bar{\nu}_j^2} = \bar{\nu}_j^2 - n_1 \frac{d\bar{\nu}_j}{dn_1}.$$

Note that the ionization behavior of protein j, as represented by the parameters z_j^0, $\bar{\nu}_j^2$ and $\overline{\bar{\nu}_j^2}$, is typically extracted from titration data for the protein.

Table 1
Protein properties for IEF simulations

pH	Net valence	
	Albumin	Hemoglobin
3.0	58	68.5
3.5	35.5	43.5
4.0	13	–
4.5	–	25.5
4.8	0.0	–
6.0	–	10.25
6.8	−12.2	–
7.0	–	0.0
7.8	−18.3	–
8.0	–	−10.25
8.8	−24.4	–
9.0	–	−20.5
10.0	−32	−37.5
11.0	–	−50
11.1	−48	–
12.0	−84	–
Diffusion coefficient (m^2/s)	$5.94 \cdot 10^{-11}$	$6.8 \cdot 10^{-11}$

Examples of such data are given in Table 1 for albumin and hemoglobin, the two proteins used in this study.

Substituting Eq. (5) and Eq. (6) into Eq. (4) yields

$$0 = -\nabla \cdot [\sigma\nabla\phi + ek_B T \sum_{k=1}^{N} \omega_k z_k \nabla n_k + ek_B T \sum_{j=1}^{M} \omega_{N+j} \nabla(z_{N+j} n_{N+j})], \tag{7}$$

where

$$\sigma \equiv e^2 \sum_{k=1}^{N} z_k^2 \omega_k n_k + e^2 \sum_{j=1}^{M} [(z_j^0)^2 - 2\bar{\nu}_j z_j^0 + \overline{\bar{\nu}_j^2}] \omega_{N+j} n_{N+j}$$

is the local electrical conductivity.

The model is made complete by writing conservation relations for the solutes, while accounting for the dissociation–association reactions that occur in the solution. For example, inasmuch as the solvent is water,

$$K_w = n_1 n_2, \tag{8}$$

if $n_2 = [OH^-]$ and $K_w = 10^{-14} M$ is the dissociation constant for water. Moreover, depending on the local pH, the ith amphoteric compound in the buffer may exist in any of three states: neutral (Am_i^0); cationic (Am_i^+); and anionic (Am_i^-). The amphoteric re-

actions are represented by mass-actions relations, viz.

$$Am_i^0 \rightleftarrows H^+ + Am_i^-$$

and

$$Am_i^+ \rightleftarrows H^+ + Am_i^0,$$

which are characterized by the equilibrium constants

$$K_i^- \equiv n_1 n_{3i+2}/n_{3i}, \quad i = 1, 2, ..., I, \tag{9}$$

and

$$K_i^+ \equiv n_1 n_{3i}/n_{3i+1}, \quad i = 1, 2, ..., I, \tag{10}$$

respectively. In Eq. (9) and Eq. (10),

$$n_{3i} = [Am_i^0], \; n_{3i+1} = [Am_i^+], \; n_{3i+2} = [Am_i^-], \quad i = 1, 2, ..., I,$$

and there are I ampholytes. The conservation equation for the ith amphoteric compound reads

$$\frac{\partial}{\partial t}[n_{3i} + n_{3i+1} + n_{3i+2}] + \nabla \cdot [\mathbf{f}_{3i} + \mathbf{f}_{3i+1} + \mathbf{f}_{3i+2}] = 0, \quad i = 1, 2, ..., I, \tag{11}$$

which accounts for ampholyte i in each of its three states of ionization. For the proteins, one proceeds similarly, arriving at the following conservation relation:

$$\frac{\partial n_{N+j}}{\partial t} + \mathbf{v} \cdot \nabla n_{N+j} = \omega_{N+j} k_B T \nabla^2 n_{N+j} + e\omega_{N+j} \nabla \cdot (z_{N+j} n_{N+j} \nabla \phi), \quad j = 1, 2, ..., M. \tag{12}$$

In contrast to the ampholytes, for which the ionization equilibria appear explicitly as mass-action relations Eq. (9) and Eq. (10), the protein ionization equilibria are subsumed in the titration data from which the effective valence z_{N+j}, etc., are obtained.

2.2. Accounting for the recycle features

Eq. (1) and Eqs. (7)–(12) are the balance laws that provide the framework for the modeling of electrophoretic separations processes. These balance laws have been extensively applied and tested in circumstances involving one-dimensional problems, where the spatial variations of the dependent variables are in the direction of the imposed electric field [18].

However, recycling electrophoretic separations are two dimensional insofar as they involve a flow that is directed transverse to the imposed electric field, as depicted in Fig. 2. The electric field is applied laterally (along the x-axis) across a distance a, known as the separation length. The fluid enters the separation chamber through the ports of an inlet manifold (not shown). Due to the action of the electric field, electrophoretic migration of the separands and the buffer constituents occurs while the fluid is in the chamber. As a consequence, the concentration profile that is removed at the top of the chamber differs from that which entered at the bottom. As the fluid exits the separation chamber, it is channeled through the ports of an outlet manifold into recycling tubes, where the influence of the electric field vanishes and local mixing of the components occurs. The recycle tubes carry the fluid around the recycle loop; heat is exchanged and gases are removed in the bubble trap. Subsequently, the fluid is reintroduced at the bottom of the separation chamber. To avoid mixing in the separation chamber, the manifold ports are aligned so that the fluid exits and renters at the same lateral position (x-coordinate). The cycling of the fluid through the separation chamber is continued until a suitable fractionation is achieved.

When applied to the fluid in the separation chamber, Eq. (12) reads

$$\frac{\partial \langle n_j \rangle}{\partial t} + \langle v_x \frac{\partial n_j}{\partial x} \rangle + \langle v_y \frac{\partial n_j}{\partial y} \rangle + \langle v_z \frac{\partial n_j}{\partial z} \rangle = \omega_j k_B T \left(\frac{\partial^2 \langle n_j \rangle}{\partial x^2} + \frac{\partial^2 \langle n_j \rangle}{\partial z^2} \right) + e\omega_j \left(\frac{\partial}{\partial x} \langle z_j n_j \frac{\partial \phi}{\partial x} \rangle + \frac{\partial}{\partial z} \langle z_j n_j \frac{\partial \phi}{\partial z} \rangle \right), \quad j = 1, 2, ..., M, \tag{13}$$

where the angled brackets denote averaging with respect to the y-coordinate, i.e.,

$$\langle \cdot \rangle \equiv \frac{1}{2b} \int_0^{2b} \cdot \, dy$$

The subscript $N+j$ has been dropped in favor of j, which is understood to refer to the jth protein, and we have made use of the fact there is no flux of

protein normal to the front ($y=0$) and back ($y=2b$) faces of the chamber.

To further simplify Eq. (13) we make several approximations. First, except perhaps near the inlet and outlet manifolds and on the ends ($x=0, L$) of the chamber, $v_y \ll v_x, v_z$, so the influence of convection in the y-direction is not significant. The convective term in the x direction is retained because, with recycling ITP, an externally-imposed flow can be directed against the isotachophoretic motion to arrest the translation of the components along the separation axis [4]. Second, since the electric field is imposed along the separation axis (i.e., in the x-direction), $\partial\phi/\partial x \gg \partial\phi/\partial z$ and electromigration in the z-direction can be neglected. Third, the Peclet number $\langle v_z\rangle L/\omega_j k_B T$ is quite large ($>10^6$), implying that convection dominates diffusion in the z-direction. That is, the strong recycling flow diminishes gradients with respect to z by spreading the solutes vertically. Accordingly, the spatial gradients along the separation axis are much larger than those in the direction of the recycling flow. Note though that concentration gradients with respect to z do exist and are important, since as the fluid moves from the bottom to the top of the chamber, the electrophoretic separation progresses – albeit a modest amount per cycle.

A final approximation is related to the mixing of solutes in the recycle loop. As the fluid cycles back around to the inlet of the separation chamber, passing through the peristaltic pump and the bubble trap (see Fig. 1), the solute concentrations tend to be averaged over the cross-section of the recycle tubes. At the inlet ($z=0$), the concentration profiles are essentially independent of y and, as noted, variations with respect to z are comparatively small within the chamber. Thus

$$\langle v_x \frac{\partial n_j}{\partial x}\rangle \approx \langle v_x\rangle \frac{\partial\langle n_j\rangle}{\partial x}, \quad \langle v_z \frac{\partial n_j}{\partial z}\rangle \approx \langle v_z\rangle \frac{\partial\langle n_j\rangle}{\partial z},$$

$$\frac{\partial}{\partial x}\langle z_j n_j \frac{\partial\phi}{\partial x}\rangle \approx \frac{\partial}{\partial x}[\langle z_j\rangle\langle n_j\rangle \frac{\partial\langle\phi\rangle}{\partial x}],$$

and we henceforth ignore variations with respect to y.

With the foregoing approximations, Eq. (13) works down to

$$\frac{\partial\langle n_j\rangle}{\partial t} + \langle v_x\rangle\frac{\partial\langle n_j\rangle}{\partial x} + \langle v_z\rangle\frac{\partial\langle n_j\rangle}{\partial z} = \omega_j k_B T \frac{\partial^2\langle n_j\rangle}{\partial x^2} + e\omega_j\frac{\partial}{\partial x}[\langle z_j\rangle\langle n_j\rangle\frac{\partial\langle\phi\rangle}{\partial x}], \quad j=1,2,...,M, \tag{14}$$

which can now be manipulated into a one-dimensional problem by adopting a frame of reference that translates with the recycle velocity $\langle v_z\rangle$. As is well known, this is done formally by defining a new z-coordinate, $z^* = z - \langle v_z\rangle t$, so that in the moving frame Eq. (14) becomes

$$\left(\frac{\partial\langle n_j\rangle}{\partial t}\right)_{x,z^*} + \langle v_x\rangle\frac{\partial\langle n_j\rangle}{\partial x} = \omega_j k_B T\frac{\partial^2\langle n_j\rangle}{\partial x^2} + e\omega_j\frac{\partial}{\partial x}[\langle z_j\rangle\langle n_j\rangle\frac{\partial\langle\phi\rangle}{\partial x}], \quad j=1,2,...,M. \tag{15}$$

The terms that remain balance the local accumulation against diffusion and electromigration, while allowing for convection along the separation axis, such as might occur with an imposed counter flow [4] or electroosmosis driven by the applied electric field. A similar result is obtained for the ampholytes, i.e.,

$$\frac{\partial}{\partial t}[\langle n_{3i}\rangle + \langle n_{3i+1}\rangle + \langle n_{3i+2}\rangle]_{x,z^*} + \langle v_x\rangle\frac{\partial}{\partial x}[\langle n_{3i}\rangle + \langle n_{3i+1}\rangle + \langle n_{3i+2}\rangle] = \omega_{3i}k_B T\frac{\partial^2}{\partial x^2}[\langle n_{3i}\rangle + \langle n_{3i+1}\rangle + \langle n_{3i+2}\rangle] + e\omega_{3i}\frac{\partial}{\partial x}\{[z_{3i}\langle n_{3i}\rangle + z_{3i+1}\langle n_{3i+1}\rangle + z_{3i+2}\langle n_{3i+2}\rangle]\frac{\partial\langle\phi\rangle}{\partial x}\}, \quad i=1,2,...,I. \tag{16}$$

Electroneutrality (Eq. (1)), the charge balance (Eq. (7)) and the ionic equilibria (Eq. (9) and Eq. (10)) are unaltered by the change of reference frame, though the dependent variables are replaced by their y-averaged values. Further note that Eq. (7) reduces to its one-dimensional form since variations with respect to x are dominant.

Eq. (15) and Eq. (16) are of the same one-dimensional form as that used by previous investigators to express solute conservation – except now we move vertically with the recycling flow. Owing to this, the influence of recycling on the mathematical structure of the problem is manifested in the conditions that must be prescribed on the concen-

tration profile as the fluid enters the separation chamber each cycle.

2.3. Initial and boundary conditions

At time $t=0$, the solute concentrations that enter the separation chamber are taken to be those introduced to the bubble traps as the device is filled preparatory to imposition of the electric field (cf. the experimental section). Hence the concentration of the kth solute

$$\langle n_k\rangle(x, 0) = n_{k0}(x), \quad k = 1, 2, ..., N+M, \tag{17}$$

is known at the inception of the separation process. As the fluid moves through the separation chamber, some fractionation of the separands occurs, governed by the balance laws outlined above. The fluid then exits at time t_S, the residence time in the separation chamber. We assume that while in the recycle loop, the solute concentrations in an individual recycle tube are averaged over the tube cross-section. Axial mixing also occurs, but after the first few cycles, this effect is small; solute concentrations vary much more from tube to tube than they do along an individual tube. If the residence time of the fluid in the recycling loop is denoted t_R, the fluid exiting the chamber at t_S, re-enters at time $t_C = t_S + t_R$, the time to complete one cycle. Our concept of this repetitive process is depicted in Fig. 3.

In general the time at the inception of cycle number n_C is $t = (n_C - 1)t_C \equiv t_{n_C}$ and the concentration profile that enters the chamber can be determined from that which exits the chamber at time $t_{n_C-1} + t_S$. Let $B_{k,l}$ represent the average concentration of solute k that emerges from the chamber at time $t = t_{n_C-1} + t_S$ and flows into recycle tube l, i.e.,

$$B_{k,l} = \frac{1}{(x_l - x_{l-1})} \int_{x_{l-1}}^{x_l} \langle n_k\rangle(x, t_{n_C-1} + t_S)\,dx, \qquad l = 1, 2, ..., N_T, \tag{18}$$

where N_T is the number of recycle tubes and $x_{l-1} \le x \le x_l$ is that portion of the chamber drained by tube l. The concentration profile introduced to the chamber at t_{n_C} is then given by

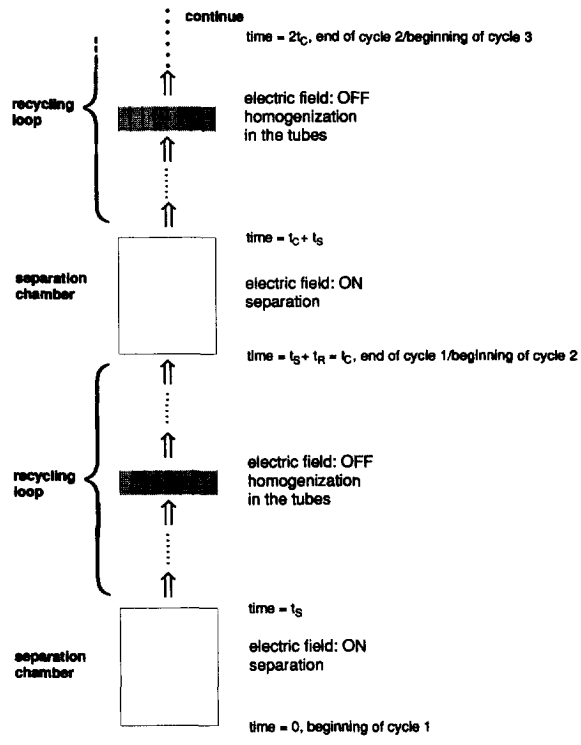

Fig. 3. Conceptualization of the operation of a recycling electrophoresis device as a series of initial value problems.

$$\langle n_k\rangle(x, t_{n_C}) = \begin{cases} n_k^{(0)} & x = 0 \\ B_{k,1} + \sum_{l=1}^{N_T-1} (B_{k,l+1} - B_{k,l})H(x - x_l) & 0 < x < a \\ n_k^{(a)} & x = a \end{cases} \tag{19}$$

where $H(x-x_l)$ is the Heaviside function [19]. The concentrations $n_k^{(0)}$ and $n_k^{(a)}$ are determined, respectively, from the boundary conditions imposed at $x=0$ and a, the lateral edges of the separation chamber. For ITP a Dirichlet condition is prescribed, viz.

$$\left.\begin{aligned}\langle n_k\rangle(0,t) &= n_k^{(0)} = n_k^{(-\infty)}\\ \langle n_k\rangle(a,t) &= n_k^{(a)} = n_k^{(+\infty)}\end{aligned}\right\} \quad k = 1, 2, ..., N+M, \tag{20}$$

while for IEF, the flux component $k_B T\partial\langle n_k\rangle/\partial x + e\langle z_k\rangle\langle n_k\rangle\partial\langle\phi\rangle/\partial x$ vanishes at $x=0, a$. We consider either constant current or constant voltage operation of the devices and these proscriptions on the problem yield the boundary condition for the electric potential [18].

2.4. Numerical approach

Except for the recycle features, the numerical solution to the balance laws has been discussed by Mosher et al. [18]. The spatial domain was discretized into uniformly-spaced grid points with the derivatives represented by three point central difference formulas; adjacent to the lateral boundaries, the appropriate forward or back differences were employed. The number of grid points per recycle tube was always some integer multiple of six, so the total number of grid points was $(6m-1)N_T+1$, with m typically equal to one, two or three. Convergence was established by comparing the solutions obtained at different values of m. The integral in Eq. (18) was evaluated with a six-point, closed Newton–Cotes formula [20].

A Runge–Kutta–Fehlberg algorithm [21] was used to take the time steps. To avoid spurious sources and sinks of material due to truncation errors, the total concentration of each solute was renormalized to the initial value every few cycles.

3. Experimental

3.1. The ITP device

The device used for the ITP experiments is a prototype of the RF3 and has been described previously [3,4]. The main component of the apparatus is a separation chamber, comprised of a thin (about 0.75 mm) flow-through duct of rectangular cross-section, formed between two parallel plates. One of the plates is a cooling block with circulating coolant. The cell is 6.5 cm wide (separation length) and 35.0 cm high. The chamber contains no supporting matrix nor compartments to guide the flow. A multichannel peristaltic pump recycles the fluid continuously from the top of the chamber through 48 PTFE tubes, reintroducing the fluid to the chamber at the bottom. The recycling loops pass through bubble traps and a heat exchanger to remove Joule heat. High flow-rates ensure hydrodynamic stability and keep the streamlines perpendicular to the applied electric field. The electric field is applied by means of platinum electrodes, located at the two sides of the chamber. The electrodes are immersed in their own compartments and separated from the main chamber by ion-exchange membranes.

The fluid in the electrode compartment is also recycled. The power is supplied by an EC600 (E-C Apparatus, St. Petersburg, FL, USA). Operation under constant voltage drop, constant power and constant current are possible. The process fluids have, per cycle, a residence time of 0.09 min in the chamber and of 0.63 min in the return loops.

3.2. The IEF device

For experiments on IEF, a prototype of a new recycling device was used (Protein Technologies). It was optimized for ease of construction, assembly and use, as shown schematically in Figs. 4 and 5. Its unique feature is the nylon monofilament screen, inserted between two sealing spacers, containing the array of separation cavities (compartments). The assembly is shown in Fig. 6 and is disposable. While the present version was geared to minimize priming volume, it can be readily scaled to larger volumes, as is common in tangential flow filtration. This method of partitioning the compartments means that the separands migrate electrophoretically between neighboring compartments in a hop-scotch fashion, passing virtually unimpeded by the screen. Thus the transport along the separation axis (x-axis) follows a tortuous, serpentine path between the electrodes. The depth of a cell compartment is 2.3 mm. The shortest distance from the anode compartment to the cathode compartment is 50 mm. The width of a subcompartment is 5 mm, the height is 50 mm. The cross-sectional area of one compartment perpendicular to the axis of separation was taken to be 0.91 cm^2. The electric field is applied across platinum electrodes,

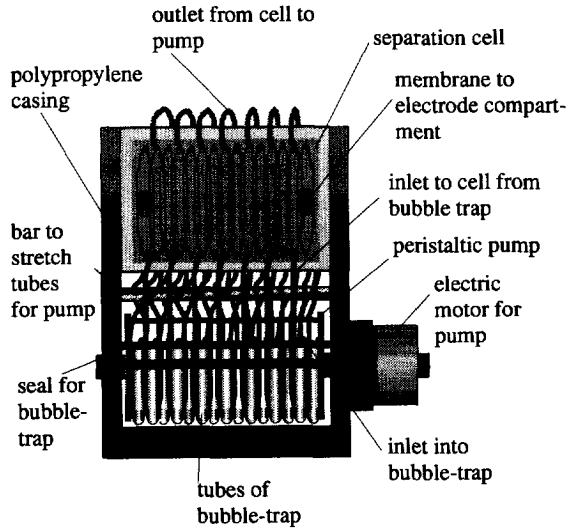

Fig. 4. Sketch of the prototype recycling free-flow IEF device used for the IEF experiments.

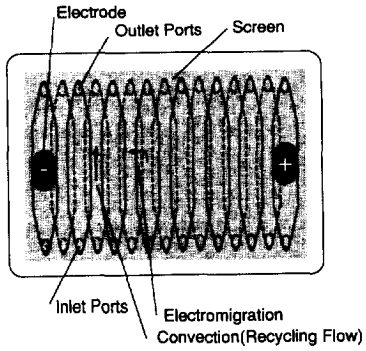

Fig. 5. Sketch of the array of separation cavities (chambers) in the IEF cell.

housed in electrode compartments and separated by dialysis membranes from the main cell. The solutions in the electrode chambers are recycled. The process fluids have per cycle a residence time of 0.075 min in the cell and of 0.24 min in the return loop. The device has a bubble trap which consists of an array of fifteen 1.5 ml Eppendorf microcentrifuge tubes, one for each of the compartments. The cell is filled and emptied through the bubble trap. The fill volume of each batch run was 22.5 ml. A peristaltic pump is used to cycle the liquid from the compartments to the bubble trap. The cycling flow-rate is 71.43 ml/min. The pump is driven by an electric motor. The voltage source is the same as that in the ITP experiments. This prototype IEF device is not equipped with a heat exchanger. For this reason, the experiments were conducted in a refrigerator.

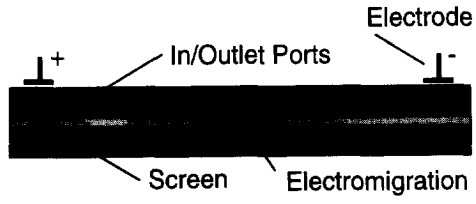

Fig. 6. Top view of the IEF cell showing the arrangement of the separation cavities (chambers) and the monofilament screen.

3.3. ITP experiments

The leader in all of the ITP experiments was 5 m*M* HCl and the terminator was 5 m*M* *p*-aminobenzoic acid (PABA). Each electrolyte was adjusted to pH 6.0 by the addition of histidine (His). To have a single moving front, the simplest possible ITP case, no components (i.e., no separands) were placed between the leader and the terminator.

The anode electrode chamber is separated from the cell by a Raypore strong anion-exchange membrane R5030H from RAI Research (Long Island, NY, USA). This membrane has been shown to have a very high permeability for PABA anions moving into the separation chamber. For the cation side, Spectrapor standard cellulose dialysis membrane tubing, with 12 000–14 000 *MW* cutoff, from Spectrum Medical Industries (Los Angeles, CA, USA) was used.

The terminator was pipetted into container 0, the cathode compartment. The 48 containers of the bubble trap for the electrophoresis chamber, as well as the reservoir for the anode, were initially filled with the leader. In the ITP experiments the cathode was on the left side. Cooling and recycling were started before the electric field was applied and the temperature was equilibrated to 4°C. The temperature was held constant during the experiments. An UV monitor was placed in recycling loop 39 to measure the optical density of the fluid. The experiment was stopped when the PABA concentration at the detection point reached 2.7 m*M*. Note recycling loop 39 (i.e., the detection point) is 5.3 cm down the

separation axis from the cathode membrane. ITP runs were done under constant voltage drop. The current, voltage and power were monitored. To avoid biasing of results (by convective remixing during the emptying of the cell) only the liquid in the bubble trap(s) was used for concentration measurements; the concentration was measured using a UV spectrophotometer (UV1600U, Shimadzu, Torrence, CA, USA).

3.4. IEF experiments

IEF experiments were conducted with a PABA–L-arginine (Arg)–cycloserine (Cyc) buffer system with each component introduced at a concentration of 4 m*M*. The buffer was initially pipetted into the receptacles that form the bubble trap, 1.5 ml into each container (except for container 8). Container 8 was filled with 1.5 ml of an albumin–hemoglobin–buffer mixture; the albumin concentration was 2.5 mg/ml and the hemoglobin concentration was 3.17 mg/ml. These proteins were selected because they separate into blue and red bands that are easy to distinguish. 0.1 *M* NaOH was used in the cathode compartment and 0.1 *M* H_3PO_4 in the anode compartment. The experiments were run in a refrigerator at 7°C. The current was held constant throughout the experiments. The voltage drop across the cell (including the electrode compartments and membranes) was monitored during the experiment. Changes in the bubble trap fluid levels were monitored to gauge the strength of any electroosmosis and to avoid the entrainment of air in the cell. In all IEF experiments the anode was on the left side of the device as portrayed in Fig. 6. The results are also shown with the anode to the left.

After each run, samples were collected in the bubble trap by reversing the peristaltic pump. The temperature was measured at the time of sample collection. Temperature increases during the experiment never exceeded 4 K.

After measuring the temperature, the bubble trap was placed in a water-bath and heated to 25°C. The conductivity of the 15 containers was then measured. Based on repeated conductivity measurements, the estimated error in these results is $1.8 \cdot 10^{-3}$ S/m. After measuring the conductivity, the pH was measured (Model 320, Corning, Corning, NY, USA) to within 0.1 pH unit.

For protein separations, concentrations were determined with a UV spectrophotometer. The process solution had to be diluted (often to 1:1000) to obtain a low enough concentration for the optical density measurement. Also, small amounts of protein were observed to coat the monofilament nylon screen, though not enough to upset the mass balance by more than a few percent.

4. Comparison of simulations with experiments

Several runs were performed to verify that the newly developed simulation strategy yields reasonable predictions of the behavior of IEF and ITP recycling. The buffer and protein properties used in the simulations are summarized in Tables 1–3.

Fig. 7 shows a separation of the two proteins, albumin and hemoglobin, after 41 min in the IEF mode, operating at constant current conditions with PABA–Arg–cycloserine buffer. This is a transient profile, which obtains about halfway to the steady state. Experiment (panel (a)) and simulation (panel (b)) show similar results, though the separation has proceeded somewhat further in the experiments. For example, the proteins peaks are more resolved. The pH range of the experiments is broader by about 1.5 units and the simulation shows a small plateau, not seen the experiments, between tube 6 and 9. Conductivity measurements (not shown) indicate that the compartments near either end of the device are affected by the electrode reactions and this probably contributes to the discrepancy in the pH range.

Fig. 8 shows the results of another IEF trial with the same system, run this time to completion (100

Table 2
Buffer properties for IEF simulations

Component	p*K* values	Mobility (10^{-8} $m^2/V s$)	Initial conc. (m*M*)
PABA	2.41/4.85	3.28	0.004
L-Arginine	9.04/12.48	2.26	0.004
Cycloserine	4.4/7.4	3.6	0.004

Table 3
Buffer properties for ITP simulation

Component	pK values	Mobility (10^{-8} m^2/V s)	Initial condition	
			Concentration (mM)	Position (cm)
HCl	–	7.91	5.0	0.3–6.5
PABA	2.41/4.85	3.28	5.0	0.0–0.3
His	6.0/9.17	2.85	9.5	0.0–0.3
			10.0	0.3–6.5

min). Each protein is focused in a single compartment, at their respective pI values. The profiles in the experiment are displaced one compartment toward the cathode and, as before, the pH range of the experiments is wider (by 2 units). During the experiment we observed a decrease in the fluid level of the bubble traps towards the anode and an increase in the level of those towards the cathode. These observations are an indication of electroosmosis in the separation chamber. The primary source of this electroosmosis would appear to be the screen between the compartments (see Fig. 6). The same experiment was also carried out with the screen removed. In that case we found no fluid level changes, but it was also impossible to focus the proteins into single compartments, inasmuch as the screen is necessary to streamline the forced convection.

Finally, a careful review of the figure shows two more subtle features. The protein concentrations introduced to compartment 8 at the inception of the experiment and simulation were 2.5 mg/ml and 3.17 mg/ml for the albumin and hemoglobin, respectively. In panel (a), one can see that the final hemoglobin concentration has diminished to 3 mg/ml. This 5% loss can be attributed to adsorption of the proteins on the screen, as well as to small errors incurred in the concentration measurements, i.e., the mass balance on the albumin appears to be closed. In panel (b), the concentrations of both proteins can be seen to have *increased*. Thus is due to the accumulation of numerical errors as the simulation scheme steps forward in time. To subsequently avoid these artificial material sources, we renormalized the total concentration of each solute in the system after every few time steps. The result of this corrective step can be seen in Fig. 17 (a), where the concentration profiles for the same simulation are shown.

ITP simulation and experiment are compared in Fig. 9, for the HCl(leader)/PABA(terminator) system. In the experiment, the leader/terminator front began at $x=0$ cm, and in the simulation at $x=0.3$ cm. Each were stopped when the terminator concentration reached 90% of the Kohlrausch value [22] at a point 5.3 cm down the separation axis from the starting position of the front. The voltage of the simulation (335 V) was selected to match the initial current of the experiments. Virtually identical results were obtained by matching the voltage of the experiments (400 V), though the front migrated approximately 20% faster. The plot inset to panel (a) is a simulation without recycling, though the time in the separation cell is the same as for the simulation with recycling. Thus the inset figure can alternatively be interpreted as a recycling simulation without remixing of the solutes in the recycle loop (correcting, of course, for the time spent outside of the chamber). The terminator profile is qualitatively the same in the simulation and the experiment. The concentration of the PABA plateau is about 22% higher than in the experiment, which may be due to mass transfer resistance offered by the cathode membrane. The gradient of the PABA front is, without remixing, almost vertical; the recycling with remixing has a dispersive effect on the fronts. This dispersion also took place in the experiment, shown in panel (b). The gradient of the PABA front is very similar to the simulated gradient with remixing. The simulation time (31 min) in (a) is about 8.8% under the experimental time – a substantial improvement over the simulation without recycling. The translation rate of the front in the experiments is slowed by

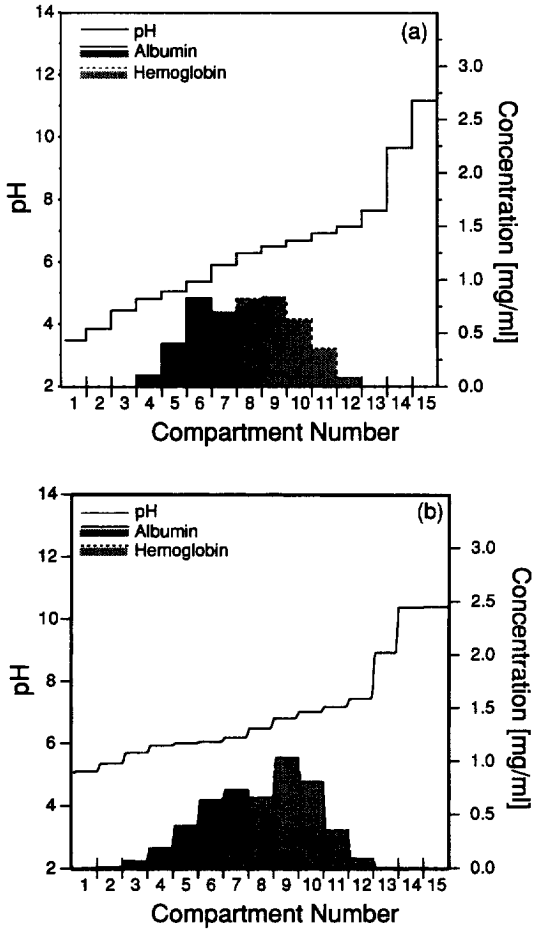

Fig. 7. Transient profiles of pH, and albumin and hemoglobin concentrations, for IEF in the PABA–Arg–cycloserine buffer system. Results shown are for 41 min of operation under constant current conditions (22 A/m^2); $N_T=15$; $t_S=0.075$ min; $t_R=0.24$ min. The anode is located to the left. Initial buffer concentrations, 4 mM each; proteins were initially introduced in compartment 8 at the following concentrations: albumin, 2.5 mg/ml; hemoglobin, 3.17 mg/ml. (a) Experimental: initial conductivity, $2.53\cdot10^{-3}$ S/m; initial pH, 5.84. (b) Simulation: initial conductivity, $2.38\cdot10^{-3}$ S/m; initial pH, 6.19.

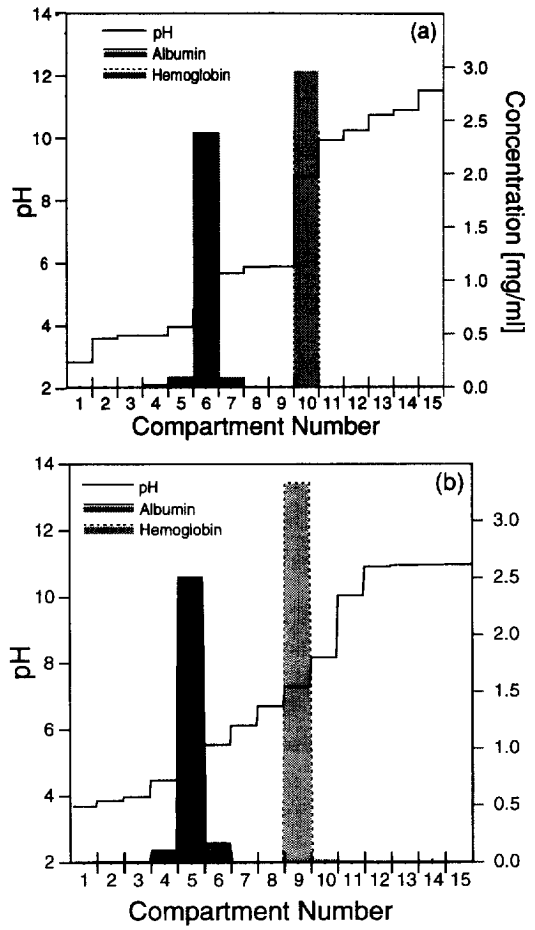

Fig. 8. Final pH, and albumin and hemoglobin concentrations, for IEF in the PABA–Arg–cycloserine buffer system ($t=100$ min). Except where noted, conditions are as for Fig. 7. (a) Experimental: initial conductivity, $2.49\cdot10^{-3}$ S/m; initial pH, 5.81. (b) Simulation: conditions are as for Fig. 7(b).

electroosmosis, which may explain some of the difference in the times.

5. Parametric studies

The above results show that the introduction of recycling with remixing to the model resulted in substantive agreement between simulations and experiments. Electroosmosis, not included in the simulation, causes a shift, but not a qualitative change in the profiles. One can account for electroosmosis as a voltage-dependent counterflow that would contribute to v_x on the left-hand side of Eqs. (15) and (16) [4].

In this section we discuss a set of parameter studies that illustrate the dynamics of recycling and are instructive for the design of new instruments. We describe the influence of three key parameters: the

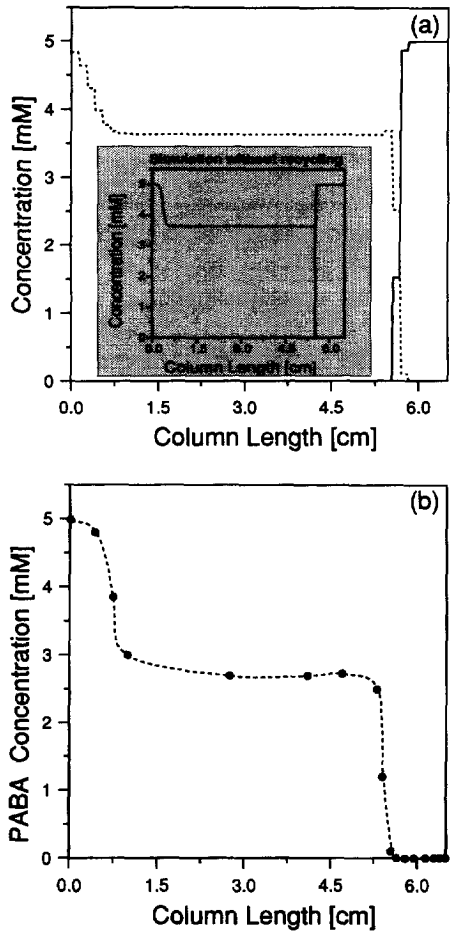

Fig. 9. (a) PABA (terminator) and HCl (leader) concentrations of constant voltage ITP simulation. Initial current density, 266 A/m^2; voltage, 335 V; t=31 min. Inset are the results after 3.4 min without recycling. (b) PABA concentration of the corresponding constant-voltage experiment after 34 min. Initial current, 266 A/m^2; voltage, 400 V; t_S=0.09 min; t_R=0.63 min. Initially, the leader and terminator concentrations are 5 mM with each adjusted to pH 5 with His; the front between the leader and terminator is initially at 0.3 cm. The cathode is located to the left and N_T=48.

number of recycle tubes; the residence time in the separation chamber per cycle; and the current density. The buffer systems and proteins used for the simulations are the same as those used in the previously discussed experiments. The ranges of parameter values that we explore are chosen so as to give a reasonable departure from the operating conditions of the prototype devices.

5.1. Effect of the number of recycling tubes, N_T

Fig. 10 shows results for the PABA (terminator) concentration profile and the width of the front as a function of the number of recycle tubes N_T. The profile for six tubes (panel (a)) shows that a Koh-

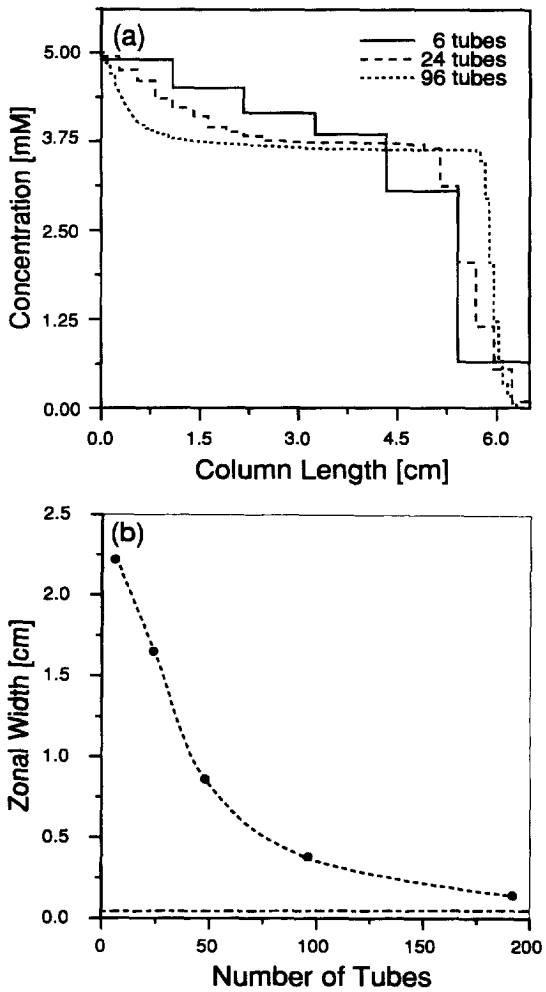

Fig. 10. Predicted influence of the number of recycle tubes on the terminator (PABA) profile in ITP. Initial buffer composition and arrangement are as for Fig. 9. Current density, 30 A/m^2 (constant); initial conductivity, $2.7 \cdot 10^{-3}$ S/m; t_S=0.09 min; t_R=0.63 min. (a) PABA profile after 31 min. (b) Zonal width of the PABA front as a function of tube number. The zonal width is the distance over which the PABA concentration varies from 0.01 mM to 3.18 mM (90% of the Kohlrausch value). The bottom line (- - - -) is the result (0.041 cm) for $N_T \rightarrow \infty$.

lrausch-adjusted concentration could not be established, as the front is spread by mixing in the recycle loops. The Kohlrausch-adjusted concentration, however, is reached with 24 or 96 tubes. The instrument used in the present study had 48 tubes and, for the buffer and voltage conditions shown, the separation length (5–6 cm) is sufficient to establish the Kohlrausch fronts. For other circumstances, however, this length will not suffice. In such instances, counterflow can be applied, making the separation length of the apparatus effectively infinite [4].

Panel (b) illustrates the effect of mixing in the recycle loop on the zone width, which is here defined as the distance over which the PABA concentration varies from 0.01 mM to 3.18 mM at the time when the leader and terminator concentrations are equal at $x=5.6$ cm. The zone width diminishes quickly – i.e., the front sharpens – as the number of recycle tubes is increased and tends asymptotically toward that obtainable in gels as $N_T \rightarrow \infty$. A related effect is seen in Fig. 11 for the migration time of the front. The migration time given in the figure is that required for the terminator to reach 90% of the Kohlrausch value at $x=5.6$ cm. The time delay with decreasing tube number is attributable to spreading of the front by mixing in the recycle loop. For both the zone width and the migration time, the parametric sensitivity is highest for small numbers of tubes since, with few tubes, the solutes become spread over nearly the whole cell.

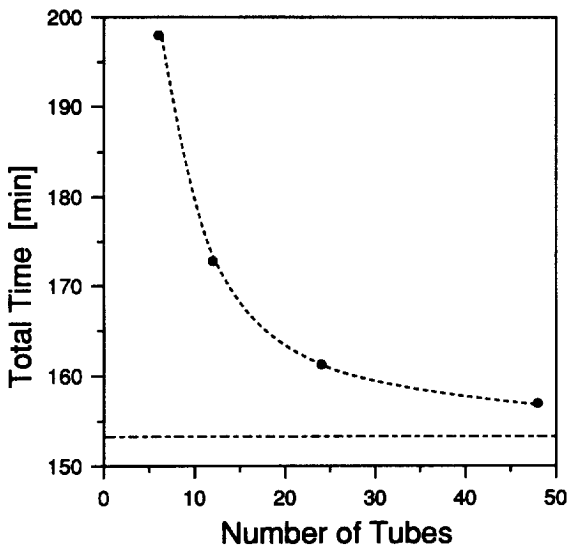

Fig. 11. Influence of the number of recycle tubes on the separation time in ITP. The time shown is that required for the terminator (PABA) concentration to reach 3.18 mM (90% of the Kohlrausch value) at $x=5.6$ cm. Conditions and initial values are as for Fig. 10. The bottom line (– – – –) is the result (153.4 min) for $N_T \rightarrow \infty$.

The effect of tube number on IEF is illustrated in Fig. 12, where the steady-state albumin and hemoglobin concentrations are shown. The current density is 5.5 A/m^2 for each simulation, so the results clearly show that the local mixing in the recycle tubes has a dispersive effect in the chamber. To make for a fair comparison between the panels, the initial condition used was the solute profile obtained after one cycle of a simulation like that for panel (c). This single cycle was started with the initial condition used for Figs. 7 and 8. Note that no fractionation could be achieved with only four tubes and, as more tubes are used, the separation approaches that obtainable in gels. Fig. 13 shows the albumin peak height and width as a function of tube numbers. The peak width is very sensitive for small tube numbers. The peak height has about the same sensitivity for all number of tubes we examined. There is a trade off between peak height/resolution and separation time, as one increases the number of recycle loops. More tubes make sharper focusing possible (at a given current density), but the time required increases substantially. The parameters are all interdependent, of course, thus an increase of current density will yield much sharper separations in a shorter time – even with 15 tubes – as shown in Figs. 8 and 17.

5.2. Influence of residence time per cycle, t_S

In sharp contrast to tube number, the ratio t_S/t_R has little effect on the leader/terminator concentration profiles for constant current ITP in the HCl/PABA system. Varying t_S/t_R from 0.036 (one quarter of the value for the experimental apparatus) to 0.571 (four times the value for the apparatus) decreased the width of the PABA front from approximately 1.3 cm to approximately 0.8 cm, and had no effect on the Kohlrausch adjusted concentrations. However, the migration rate of the leader/terminator front is a strong function of t_S/t_R, particularly if $t_S/t_R<0.10$. Fig. 14 shows that the primary effect of decreasing

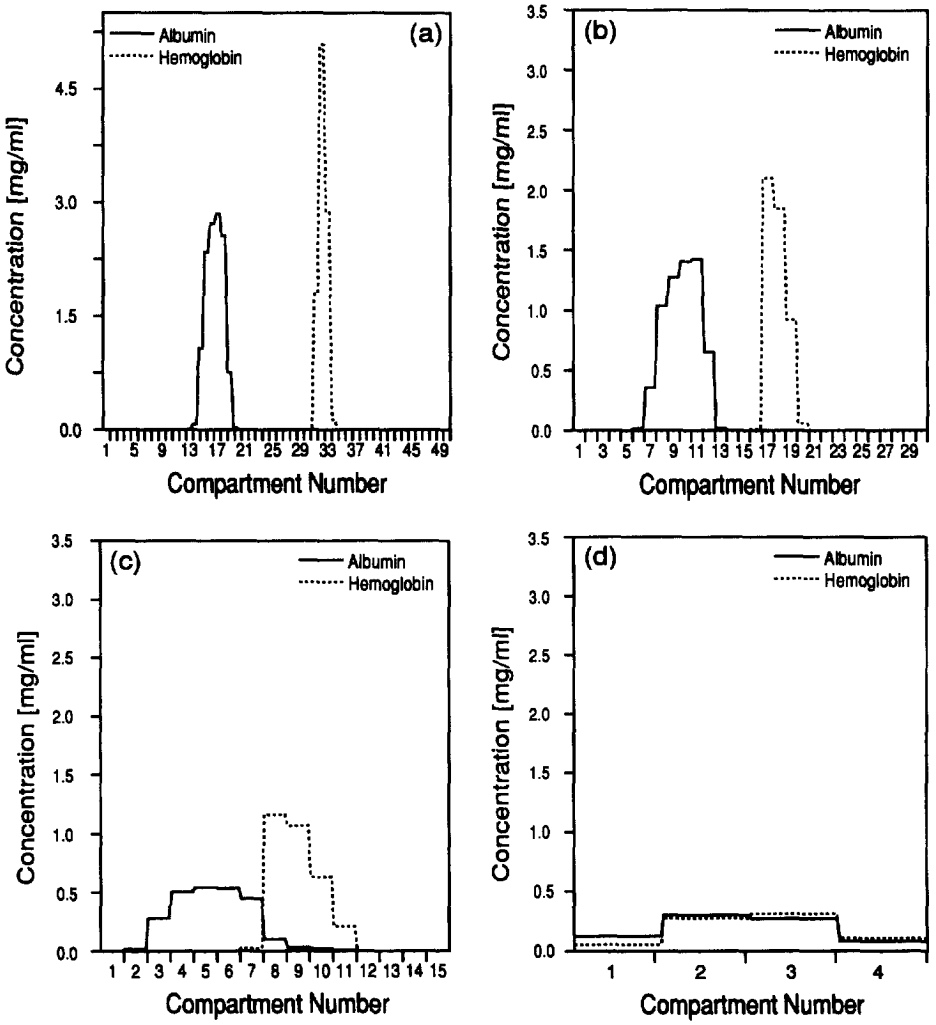

Fig. 12. Predicted steady state albumin and hemoglobin concentrations as a function of the number of tubes for constant current IEF in the PABA–Arg–cycloserine buffer system. Current density, 5.5 A/m^2; $t_S = 0.075$ min; $t_R = 0.24$ min. Initial buffer conditions are as for Fig. 7(b) and Fig. 8(b). For the four cases shown, the time to reach steady state is: (a) 1040 min, $N_T = 50$; (b) 768 min, $N_T = 30$; (c) 277 min, $N_T = 15$; (d) indeterminate due to slow temporal oscillations in the simulation, $N_T = 4$. Note that, in contrast to Fig. 8(b), the results shown in panel (c) for $N_T = 15$ indicate that complete resolution of the components is not achieved at these lower current densities.

t_S/t_R is to dilate the total time for the front to migrate. The total residence time in the separation chamber is insensitive to t_S/t_R, so the migration rate is largely a function of the time that the fluid has to spend in the recycle loop. The parameter t_S/t_R is equal to the ratio of fluid volume in the separation chamber to that in the recycle loop, including the heat exchanger and bubble traps. It would appear then from the results that, for the separation to proceed apace, the chamber should hold at least 10–15% of the total volume of fluid to be processed.

The ratio t_S/t_R affects both the rate and the outcome of IEF. Fig. 15 shows final albumin profiles as a function of t_S/t_R. For the experiments performed with the prototype IEF device (Figs. 4–6), $t_S/t_R = 0.313$. The simulations show that the number of

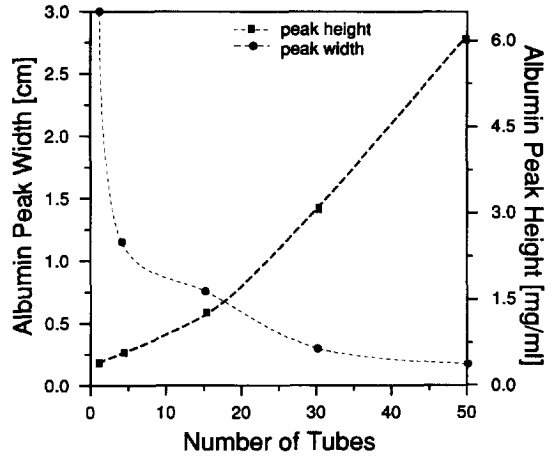

Fig. 13. Predicted final albumin peak width and height as a function of the number of tubes for constant current IEF in the PABA–Arg–cycloserine buffer system. Components and conditions as for Fig. 12. The peak width is the width at half of the maximum albumin concentration.

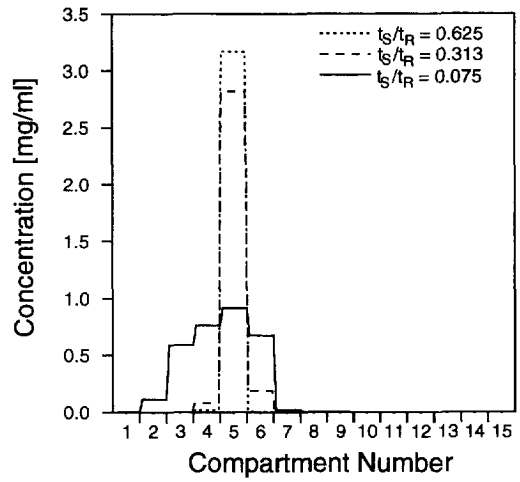

Fig. 15. Influence of t_S/t_R on the steady state albumin concentration for IEF at constant current. Buffer and operating conditions as for Fig. 12, except that the concentration of albumin introduced to compartment 8 at the inception of the simulation is now 3.17 mg/ml. For the three cases shown, the time to reach steady state is: 58.5 min (150 cycles), $t_S/t_R = 0.625$; 99.3 min (315 cycles), $t_S/t_R = 0.313$; 344.1 min (1330 cycles), $t_S/t_R = 0.075$.

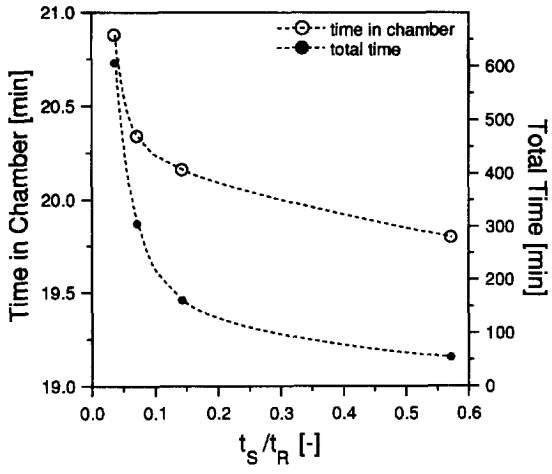

Fig. 14. Total time and time in separation chamber as a function of t_S/t_R for ITP at constant current. Conditions: current density, 33 A/m^2; $N_T = 24$; initial leader (HCl) and terminator (PABA) concentrations, 5 mM adjusted with His to pH 5; front between leader and terminator initially at 0.3 cm; initial conductivity, $2.7 \cdot 10^{-2}$ S/m. Times quoted are those required for PABA concentrations to reach 3.18 mM (90% of the Kohlrausch concentration) at $x = 5.6$ cm.

cycles required to reach the steady state varies more or less inversely with t_S/t_R. As t_S/t_R diminishes, the protein peaks broaden since there is an increase in the influence of the dispersive effects associated with mixing in the recycle loops. Thus the separation time decreases and the resolution increases with t_S/t_R. For the system depicted in Fig. 15, other simulations (not shown) reveal that the proteins are reasonably well focused for $t_S/t_R \geq 0.15$, although to concentrate the albumin completely into one compartment, t_S/t_R must exceed 0.6. While the resolution will obviously vary depending on the separands, the buffer system, and the current density, it would appear that the separation chamber should hold at least 10–15% of the total fluid volume to be processed.

5.3. Effect of the current density

The last parameter that we consider for study is current density. Because chamber residence times are typically far less than a minute, and because re-

cycling devices allow for better temperature control, the effects of Joule heating are not problematic. This allows one to employ stronger electric fields to bring about a separation.

Fig. 16 shows the effect of current density on the width and migration time of the PABA front in constant current ITP. The ITP experiments with this leader/terminator system were done at constant voltage (see Fig. 9), where the current density ranged from 266 A/m^2 at the inception, down to 133 A/m^2 as the front reached $x=5.3$ cm. Here the simulations are for current densities below those of the ITP experiment. The results show that, above 50 A/m^2, the terminator profile is comparatively less sensitive to current increases, as is also evident for the migration time. We have also found that the migration rate of the front is roughly linear in the current density, provided that the current is sufficient to produce a sharp front (i.e., above 50 A/m^2). This points to one of the attractive features of recycling ITP for preparative separations: one can use electric fields in excess of that required to produce sharp concentration fronts and thereby enhance the rate of the separation.

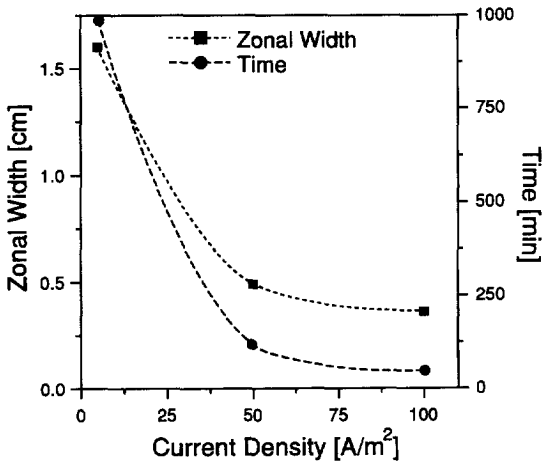

Fig. 16. Width and migration time of the PABA (terminator) front as a function of current density in ITP. Conditions are as for Fig. 10, except $N_T=48$. Zonal width is the distance over which the PABA concentration varies from 0.01 mM and 3.18 mM at the time when the leader and terminator concentration are equal at $x=5.6$ cm. The time quoted is that required for the PABA concentration to reach or exceed 3.18 mM (90% of the Kohlrausch concentration) at $x=5.6$ cm.

Fig. 17 shows the steady state albumin and hemoglobin profiles in constant current IEF. As one would expect, the resolution increases with current density. The experiments on this system were carried out at 22 A/m^2 (see Fig. 8), which, according to the simulations, is (nearly) the optimum current density. Further increasing the current density does reduce the processing time (not shown), though no such experiments were attempted.

6. Conclusions

The model formulated here indicates that the postulated mixing of solutes in the recycle loop is manifested as a dispersion that can affect the resolution of recycling electrophoresis devices. Another effect of the recycling is to slow the separation process inasmuch as fluid spends time outside of the separation chamber. This slowing of the dynamics should be weighed against the fact that one is also processing larger volumes, so the amount of material processed per unit time is not necessarily diminished in any significant way (if at all). Furthermore, because of the recycling scheme, strong electric fields can be used to enhance the rate processes.

For preparative separations, the most important implication of the model would seem to be that, while the window of operating conditions may be robust, the separation processes can become quite inefficient outside of this window. An example of this would be that, for the ITP system described, if the volume of the separation chamber becomes too small relative to the volume of fluid to be processed, the time to set up the Kohlrausch fronts grows prohibitively long – other factors being equal, of course. Because it is impossible to generalize the trends elucidated here to all buffers and separands, the utility of the simulations is to establish the certain conditions that will yield efficient separation, as well as to explore device innovations that can lead to superior performance.

Finally, it is important to recognize that there are two aspects of optimizing the resolution of a popula-

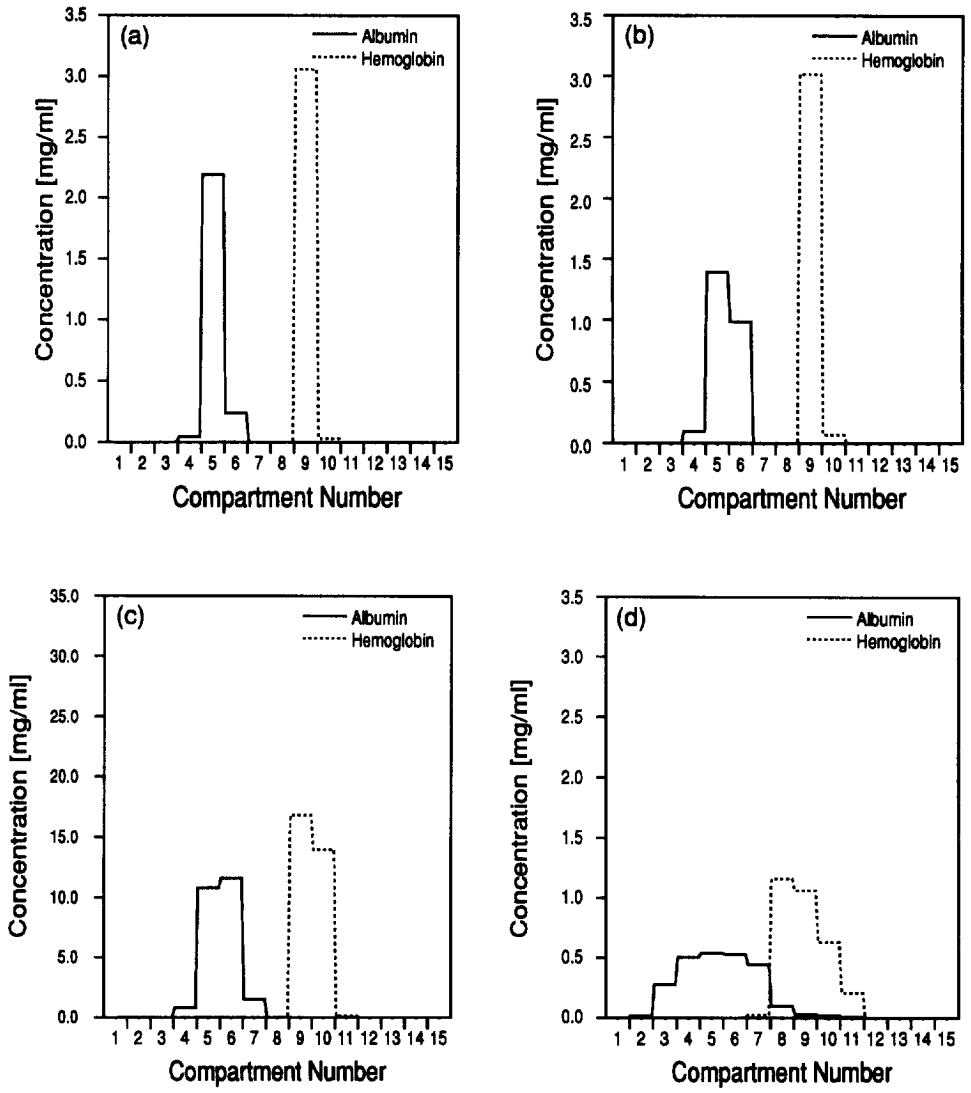

Fig. 17. Predicted steady-state albumin and hemoglobin concentration as a function of the (constant) current density in IEF. Except where, conditions are as for Fig. 8; $t_S = 0.075$ min; $t_R = 0.24$ min; initial conductivity, $2.18 \cdot 10^{-3}$ S/m; initial pH, 6.19; $N_T = 15$. (a) 22.0 A/m^2, 92.3 min; (b) 16.5 A/m^2, 117.5 min; (c) 11.0 A/m^2, 151.2 min; (d) 5.5 A/m^2, 277.2 min.

tion of separands. One involves issues such those discussed in this work, which pertain to the design and operating conditions of the electrophoretic device. The second involves the buffer in which the separation is effected. While we have not investigated the role of the buffer system in this work, such issues have been discussed by Bier et al. [23].

Acknowledgments

The authors thank Protein Technologies, Inc. for the use of the prototype IEF device and acknowledge Dr. R.A. Mosher for his assistance with the implementation of the subroutine used to describe the electrophoretic and ionogenic behavior of proteins.

References

[1] M. Bier, N.B. Egen, T.T. Allgyer, G.E. Twitty and R.A. Mosher, in E. Gross and J. Meienhofer (Editors), Peptides: Structure and Biological Function, Pierce, Rockford, IL, 1979.

[2] M. Bier, G.E. Twitty and N.B. Egen, in H. Itirai (Editor), Electrophoresis '83, Walter de Gruyter, Berlin, 1984, pp. 547–550.

[3] M. Bier, G.E. Twitty and J.E. Sloan, J. Chromatogr., 470 (1989) 369–376.

[4] R.R. Deshmukh and M. Bier, Electrophoresis, 14 (1993) 205–213.

[5] P.G. Righetti, E. Wenisch and M. Faupel, J. Chromatogr., 475 (1989) 293–309.

[6] P.G. Righetti, E. Wenisch, A. Jungbauer, H. Katinger and M. Faupel, J. Chromatogr., 500 (1990) 681–696.

[7] Z.S. Horvath, G.L. Corthals, C.W. Wrigley and J. Margolis, Electrophoresis, 15 (1994) 968–971.

[8] J. Margolis, G.L. Corthals and Z.S. Horvath, Electrophoresis, 16 (1995) 98–100.

[9] M. Bier, O.A. Palusinski, R.A. Mosher and D.A. Saville, Science, 219 (1983) 1281–1287.

[10] D.A. Saville and O.A. Palusinski, AIChE J., 32 (1986) 207–214.

[11] R.A. Mosher, D. Drewey, W. Thormann, D.A. Saville and M. Bier, J. Am. Chem. Soc., 61 (1989) 362.

[12] S.V. Ermakov, O.S. Mazhorova and Yu.P. Popov, Informatica, 3 (1992) 173–197.

[13] S.V. Ermakov, M.S. Bello and P.G. Righetti, J. Chromatogr. A, 661 (1994) 265–278.

[14] O.A. Palusinski, T.T. Allyger, R.A. Mosher, M. Bier and D.A. Saville, Biophys. Chem., 13 (1981) 193–202.

[15] M. Bier, R.A. Mosher and O.A. Palusinski, J. Chromatogr., 211 (1981) 313–335.

[16] O.A. Palusinski, M. Bier and D.A. Saville, Biophys. Chem., 14 (1981) 389–397.

[17] O.A. Palusinski, A. Graham, R.A. Mosher, M. Bier and D.A. Saville, AIChE J., 32 (1986) 215–223.

[18] R.A. Mosher, D.A. Saville and W. Thormann, The Dynamics of Electrophoresis, VCH, Weinheim, 1992.

[19] R.L. Street, Analysis and Solution of Partial Differential Equations, Brooks/Cole, Monterey, CA, 1973.

[20] B. Carnahan, H.A. Luther and J.O. Wilkes, Applied Numerical Methods, Wiley, New York, 1969.

[21] H.A. Watts, Trans. Soc. Computer Simulation, 1 (1985) 15–25.

[22] F. Kohlrausch, Ann. Phys., 62 (1897) 209–239.

[23] M. Bier, J. Ostrem and R.B. Marquez, Electrophoresis, 14 (1993) 1011–1018.